Performances of Atmospheric Correction Processors for Sentinel-2 MSI Imagery Over Typical Lakes Across China

Sijia Li, Kaishan Song, Yong Li, Ge Liu, Zhidan Wen, Yingxin Shang, Lili Lyu, and Chong Fang

***Abstract*—The launched MultiSpectral Instrument (MSI) equipped on Sentinel-2 satellites offers a powerful tool for observing the biogeochemical parameters of inland waters on a large scale. The proper use of atmospheric correction processors is essential for acquiring accurate satellite remote-sensing reflectance and downstream products. Therefore, we compared the performances of typical atmospheric correction processors, such as Sen2Cor, C2RCC-nets, C2RCC-C2X, Acolite, iCOR, Polymer, SeaDas/l2gen, and 6S processors, for MSI imagery over lake groups ($N = 296$) across China collected from 2016 to 2020. Linear fitting between corrected reflectance and *in situ* spectral measurements was used to assess performance; for the single lake, we additionally evaluated the performance of atmospheric correction processors in typical Chagan Lake in 2021. For large-scale lake groups with different water quality backgrounds, the SeaDas/l2gen and C2RCC processors performed best for all band match-ups, and the C2RCC processor had the smallest errors. The SeaDas/l2gen processor works well for the signal bands (490, 560, 665, 704, and 740 nm), followed by the signal bands (560, 665, and 704 nm) of the C2RCC processor. For large-scale observations, this study revealed that Sentinel-2 satellite optical MSI imagery related to the C2RCC processor can be used to monitor aquatic systems with high-frequency investigations. For the signal band, the SeaDas/l2gen processor was used to select potential match-ups for the availability of MSI data related to the empirical models of processors. Our results may help satellite users select appropriate atmospheric correction processors for large-scale lake observations.**

***Index Terms*—Atmospheric correction, case 2 regional coast color (C2RCC), processors, SeaDas/l2gen, Sentinel-2.**

Manuscript received 31 August 2022; revised 31 October 2022 and 25 December 2022; accepted 14 January 2023. Date of publication 24 January 2023; date of current version 21 February 2023. This work was supported in part by the National Key Research and Development Program of China under Grant 2021YFB3901101, in part by the National Natural Science Foundation of China under Grant U2243230, Grant 42201414, Grant 42171374, Grant 42071336, Grant 42171385, Grant 42101366, Grant 42201433, and Grant 42001311, in part by the Cooperation Project of Jilin Province and CAS under Grant 2021SYHZ0002, in part by the Development and Reform Commission of Jilin Province under Grant 2021C044-2, in part by the China Postdoctoral Science Foundation under Grant 2020M681056, in part by the 'Young support talents program' for Dr. Sijia from the Science and Technology Association of Jilin Province, and in part by the Land Observation Satellite Supporting Platform of National Civil Space Infrastructure Project (CASPLOS-CCSI). *(Sijia Li is first author.) (Corresponding authors: Kaishan Song; Yong Li.)*

The authors are with the Northeast Institute of Geography and Agroecology, Chinese Academy of Sciences, Changchun 130102, China (e-mail: lisijia@iga.ac.cn; songkaishan@iga.ac.cn; liyong@iga.ac.cn; liuge@iga.ac.cn; wenzhidan@iga.ac.cn; shangyingxin@iga.ac.cn; lvlili@iga.ac.cn; fangchong@iga.ac.cn).

This article has supplementary downloadable material available at https://doi.org/10.1109/JSTARS.2023.3238713, provided by the authors.

Digital Object Identifier 10.1109/JSTARS.2023.3238713

I. Introduction

EXISTING instances that quantify water quality by satellite sensors are run according to a routine process such as preprocessing imagery, extracting reflectance signals, atmospheric correction, retrieval algorithms, and downstream products, whereas new instances are picked up using cloud platform operations and level-3 surface reflectance products [1]. Most of the signals obtained above water bodies by satellite sensors originate from the atmosphere [2], [3]. For top of atmosphere (TOA) products, compensation for usable water surface reflectance signals at the air-water interface (i.e., sky glint and sun glint) is critical [4], [5], [6]. Regarding the TOA products or simple Rayleigh-corrected quantities, the main difficulty of ac comes from extracting a slight water reflectance signal, especially over productive and optically complex waters. Consequently, a variety of robust ac processors have been developed to obtain reliable water component signals for satellite-based approaches [7]. Although some oceanic ac processors with a mean sea level height and the NIR black-pixel assumption are currently being developed, they are not applicable to inland waters [8], [9], [10]. Owing to the interference produced by adjacency effects and the aforementioned sun glint, the processing of ac processors might become more difficult [11], [12]. Different processors are required to achieve the threshold criterion of 30% reflectance error across all bands of sensors according to the Global Climate Observing System [7]. The use of ac processors for inland waters to obtain accurate satellite-derived aquatic reflectance remains challenging [13], [14].

In essence, sensor design, atmospheric surface parameters, and ac processors all have a significant impact on the quality of water surface reflectance [15]. The MultiSpectral Instrument (MSI) onboard the Sentinel-2 satellite has recently sparked the attention of the scientific community in water quality mapping [11], [16], [17], [18], [19], [20]. The free acquisition of image data at resolutions of 10 m $\times$ 10 m at nadir by the Copernicus Sentinel-2 satellites has spurred applications for small-area inland waterways [7], [21], [22]. In addition, the integrated red and red edge bands may have more advantages in quantifying synthetic indicators such as the trophic state index [22]. It is provided with narrow ($<$10 nm) spectral bands in the 380–780 nm and near-infrared regions, which are the most optically active substance domains [23], as well as have a nominal revisit time of 3–5 days [24]. In particular, the European Space Agency

(ESA) officially provides the Sen2Cor processor and case 2 regional coast color (C2RCC) processor, of which the latter was designed for water bodies in Sentinel-2 toolboxes [25]. Although these conveniences for the use of bottom of atmosphere (BOA) products of the MSI sensor were provided directly, the performance of these processors was unstable or unappreciated for all types of inland water bodies [13], [14]. ESA, in coordination with the Copernicus Global Land Service program, conducted an iCOR exercise and water quality product generation (e.g., trophic state index, turbidity, etc.) with global scales for MSI imagery, except for Sen2Cor and C2RCC processors. Hence, the current results related to water quality products diverge depending on the research sites of interest and ac processors [7]. It is not sufficient to consider only the differences between the ac processors for the MSI sensor. Consequently, it is essential to choose an appropriate ac processor for product quality, which requires various application scenarios and performance evaluations.

When aerosol characteristics are obtained first, the Rayleigh-aerosol interactions and diffuse transmittances can be calculated and adjusted [7]. Because of their different optical and spatiotemporal variability, aerosol concentration and scattering reflectance are key uncertainties in satellite data [7], [9], [26], [27], [28], [29]. The analysis process leads to inconsistent performance. For MSI imagery, ESA and National Aeronautics and Space Administration (NASA) jointly conducted an Atmospheric Correction Intercomparison exercise with global datasets, including some from Beijing, China [4], [7]. None of these studies took into account the productive optical complexity of Chinese inland waters and atmospheric components, suggesting a need for large-scale observations.

In light of these difficulties, a comprehensive evaluation of ac processors applied to MSI images under large-scale observations, which is currently lacking for Chinese lakes, is necessary. Several ac processors are available for satellite-based sensors that can be divided into image-based approaches (e.g., Sen2Cor and Acolite), atmospheric radiative transfer code-based approaches (e.g., 6S), and machine learning-based approaches (e.g., C2RCC). Image-based techniques for MSI images demonstrate an advantage in places where there is no external atmospheric information [3]. Prior knowledge of the atmospheric characteristics (e.g., aerosol optical depth, water vapor, and ozone) coinciding with the satellite overpass was processed using a well-established 6S processor [3]. A machine learning-based approach, for example, using the back propagation model of the C2RCC processor, is data-driven and uses huge datasets collected from *in situ* and simulation measurements [30]. The performance of the processors is mainly determined by whether the optical characteristics of the regions of interest match the ranges of the datasets. Considering the growing requirements of novel processors or already-implemented processors, enhanced performances are yet to be investigated for different locations and optical water types [31], [32], [33], [34].

Considering the uncertainties in atmospheric correction processes, it is necessary to specify which robust processor(s) could provide more reliable reflectance for lake groups, increasing the detection of subtle variability in aquatic ecosystems [35], [36]. The purpose of this study is to identify the best-performing ac processors for MSI match-up selection and the statistical metrics employed for performance assessments. We evaluated different ac processors, such as Polymer, Acolite, iCOR, C2RCC, Sen2Cor, 6S, and SeaDas/l2gen, applied in typical lakes with different optical characteristics and water qualities. Additionally, we discuss how uncertainties in reflectance manifest in large-scale observations, followed by a description of the *in situ* data employed in the analysis. Our results and implications can help improve the feasibility of ac processors for inland lake ecosystems while paying close attention to downstream products.

II. Materials and Methods

A. Site Description

China has a highly complex terrain and various land surface features, and the climate and anthropogenic activities are unbalanced, with dense populations concentrated southeastward. The majority of the lakes are found on the Tibet-Qinghai Plateau [37]. Different lakes across China were selected and analyzed because of their wide range of biogeochemical characteristics, optical water types, altitudes, and climate zones (Fig. 1 and Table I). The boreal, alpine, high-altitude plateau, plain, volcano-dammed, and large reservoirs were classified considering geographical and environmental variability.

B. Sampling Processes

In situ measured data were collected during ice-free periods (April to October) with a GPS receiver to record location information (Table I). Lake samples (0.5 m below the water surface) distributed in the plateau, plain, and volcano were collected from 2017 to 2020. During the sampling processes, they were then placed in 2-L amber high-density polyethylene bottles, which had to be acid-cleaned. Remote lakes located at the Tibet-Qinghai had to be filtered through Whatman GF/F glass microfiber filters and filled into brown plastic bottles during fieldwork. The filtered samples and filters were stored in a portable refrigerator (4 °C) powered by field trip vehicles and brought to the laboratory within 24 h. Most biogeochemical parameters such as chlorophyll-a ([Chl-a]) were analyzed immediately. Furthermore, samples of Chagan Lake (CG1) collected on May 26th, July 18th, August 18th, and September 17th 2021 were used as additional data to evaluate the performance of ac processors with respect to a single lake (Fig. S1). These samples were collected at a fixed location every time.

C. Water Color Radiometry

Radiometric measurements were conducted within a 3 h interval (10:00 A.M.–13:00 P.M.) to avoid the potential impact of specular reflection (glint) at low sun angles, with less cloud coverage ($<5\%$) and wind speed (<3 m s^{-1}). *In situ* radiometric measurements were performed with an ASD spectrometer to acquire the upwelling radiance and downwelling irradiance from 350 to 900 nm at 1 nm increments. We first measured reflectance

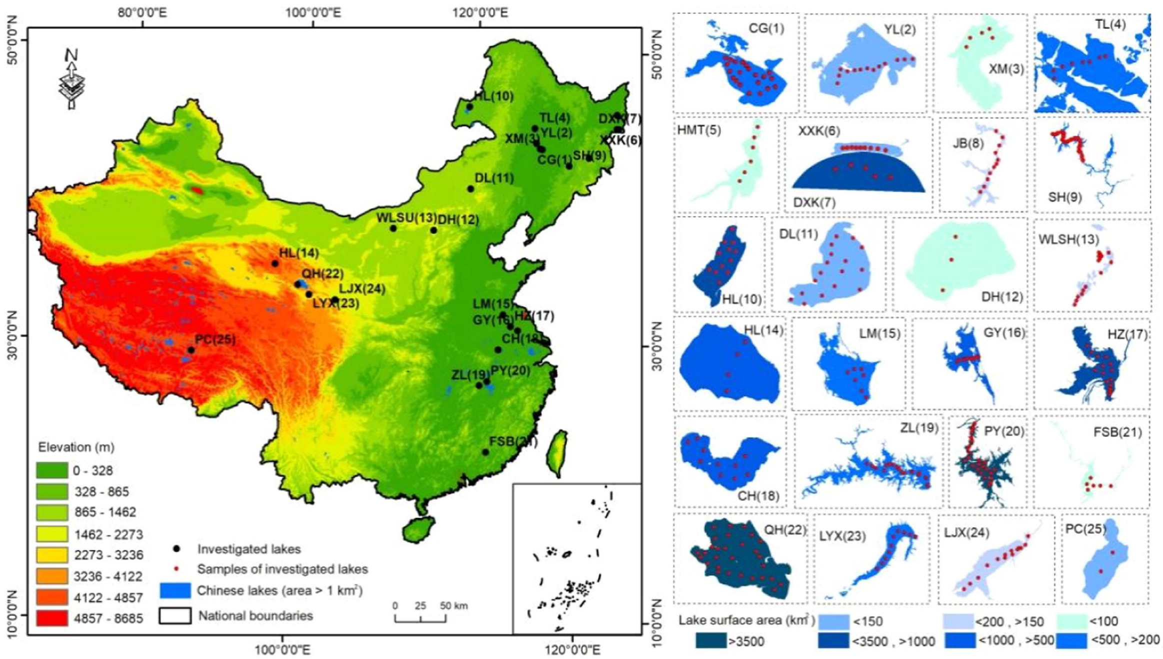

Fig. 1. Locations of studied Chinese lakes together with the sampling stations.

TABLE I
LIMNOLOGICAL CHARACTERISTICS OF THE STUDIED LAKES ACROSS CHINA

Lake names	Code	Location		Fieldwork date (yy/mm/dd)	Elevation(m)	*N*
		E	N			
Chagan Lake	CG(1)	124.27	45.28	2019/09/26; 2020/07/22; 2020/08/21	109	37
Yueliang Lake	YL(2)	124.00	45.72	2020/10/19	133	13
Xinmiao Lake	XM(3)	124.48	45.21	2020/10/18	126	5
Tala Lake	TL(4)	124.15	46.79	2020/09/11	141	8
Hamatong Lake	HMT(5)	132.86	46.32	2020/10/14	116	6
Xiaoxingkai Lake	XXK(6)	132.43	45.36	2018/10/19	54	9
Daxingkai Lake	DXK(7)	132.62	45.31	2018/10/18	53	5
Jingpo Lake	JP(8)	128.93	43.88	2018/10/16; 2020/10/16	342	20
Songhua Lake	SH(9)	126.78	43.66	2020/10/20	244	19
Hulun Lake	HLH(10)	117.63	49.11	2020/09/07	612	12
Dali Lake	DL(11)	116.68	43.24	2019/07/07	1249	10
Daihai Lake	DH(12)	112.66	40.55	2019/08/29	1408	3
Wuliangsuhai Lake	WLSU(13)	108.76	40.85	2019/08/31	1022	11
Hala Lake	HL(14)	97.597	38.20	2019/09/10	4080	4
Luoma Lake	LM(15)	118.21	34.07	2019/04/22	25	7
Gaoyou Lake	GY(16)	119.28	32.79	2019/11/05	7	10
Hongze Lake	HZ(17)	118.72	33.16	2019/08/01; 2019/11/06	6	8
Chaohu Lake	CH(18)	117.37	31.66	2019/04/20	14	10
Zhelin Reservoir	ZL(19)	115.42	29.26	2019/07/29; 2019/11/03	55	14
Poyang Lake	PY(20)	116.13	29.50	2019/04/19; 2019/07/29	143	27
Fengshuba Lake	FSB(21)	115.41	24.44	2019/11/01	146	6
Qinghai Lake+	QH(22)	99.813	36.83	2019/09/21	3178	29
Longyangxia	LYX(23)	100.85	36.16	2019/09/12	2572	8
Liujiaxia	LJX(24)	103.24	35.85	2017/09/08	1688	14
PengCo	PC(25)	90.95	31.44	2017/08/20	4535	1

+ indicates brackish waters

TABLE II
LIST OF WIDELY USED NOTATIONS, ACRONYMS, AND SYMBOLS

Symbol	Description
ρ_{w}	In situ aquatic reflectance
ρ_{s}	Satellite derived aquatic reflectance
ρ_{TOA}	TOA reflectance
ρ_{rc}	Rayleigh-corrected reflectance
[Chl-a]	In situ chlorophyll-a concentration
[TSM]	In situ Total suspended matter concentration
$a_{\mathrm{CDOM}}(440)$	In situ absorption of CDOM at 440 nm

as the ratio of upwelling radiance (L_{w}^{+0}) to downwelling irradiance (E_{d}^{+0}) above the water surface, and then measured the upwelling radiance with a 5 cm black plastic tube surrounding the sensor just below the water surface. The first measurement gives us a reflectance that contains sun and sky glint (L_{sky}^{+0}), whereas the second measurement gives the amount of true water leaving the signal as the glint is blocked by the plastic tube. Referring to Mobley (1999) [38], L_{w}^{+0} has a relative azimuth angle (φ_{v}, 90°–135°) from the sun and a zenith angle of $\theta_{\mathrm{v}} =$ 45° from the nadir, whereas L_{sky}^{+0} has a zenith angle θ_{v}'of 90° from the nadir. Ten spectra were measured at each station, and the results were averaged. A total of 296 hyperspectral remote sensing reflectances consistent with the biogeochemical parameters of the lake samples were computed, and their specific locations are shown in Fig. 1. The remote sensing reflectance ρ_w was calculated at each sampling station using the following equations:

$$R_{rs}\left(\theta_v, \varphi_v, \lambda\right) = \left(\frac{L_w^{+0}\left(\theta_v, \varphi_v, \lambda\right) - r_{sky}\left(\theta_v, \varphi_v, \lambda, w\right) \times L_{sky}^{+0}\left(\theta_v, \varphi_v, \lambda\right)}{E_d^{+0}\left(\lambda\right)}\right) \tag{1}$$

$$\rho_w = \pi \times R_{rs}\left(\theta_v, \varphi_v, \lambda\right) \tag{2}$$

where r_{sky} is the air-water interface reflection coefficient that reduces the skylight effects. The r_{sky} is a function of a given view zenith and azimuth angles ($\theta_{\mathrm{v}}, \varphi_{\mathrm{v}}$) sun zenith angle ($\theta_0$) and wind speed w (m s^{-1}) where π has units of steradian [39]. The *in situ* ρ_w spectra were convolved with those of MSI by spectral response functions to obtain band-equivalent ρ_w, which could be comparable to atmospherically corrected MSI reflectance from imagery.

D. Laboratory-Measured Biogeochemical Parameters

The main water qualities, such as chlorophyll a, total suspended matter, and CDOM, of lake surface water samples were determined (Table II). The [Chl-a] concentration (μg L^{-1}) was measured spectrophotometrically at wavelengths of 750, 663, 645, and 630 nm from 90% ethanol extracts of the filters collected during fieldwork under dimmed light conditions [40]. The total suspended matter ([TSM], mg L^{-1}) was determined gravimetrically using precombusted Whatman GF/F filters (0.7-μm pore size). For the determination of CDOM, 1-L bulk samples were filtered through Whatman GF/F filters (0.7-μm pore size) and precombusted (500 °C) for 3 h in a muffle furnace. They were then filtered through 0.2-μm pore size Whatman GF/F nuclepore filters under a gentle vacuum (<5 in Hg). The optical density of the CDOM (filtered) absorption was measured using a UV–Vis spectrophotometer at wavelengths ranging from 200 to 800 nm using a 1 cm quartz cuvette with Milli-Q as the blank and reference. The value at 440 nm was selected as the measure of the CDOM quantity [41].

E. Sentinel-2 Multispectral Instrument Imagery Data

The Sentinel-2A and B satellites currently in Earth's orbit are, respectively, loaded with the MSI, having been launched in 2015 (satellite A) and 2017 (satellite B). Thirteen spectral bands from visible to short-wave infrared were included in the MSI data, as well as spatial resolution (10, 20, and 60 m) and 12-bit quantization [42] (Table SI). These twin polar-orbiting satellites provide a 5-day revisit time of the equator and almost every second day revisit time of the high-latitude regions because they are phased at 180° to each other. These parameters are not optimal for water remote sensing, but they are the best sensors that are currently available for studying small lakes. Since 2015, MSI imagery has been available via the ESA Copernicus Open Access Hub, together with Level-1C products and TOA reflectance. The calibrated radiometrically Level-1C products were corrected for viewing geometry and orthorectified into Universal Transverse Mercator projection with the WGS84 datum. A match-up dataset of ground- and satellite-derived data was evaluated for the majority of lake samples with a time window of 7 days [43]. A total of 34 Level-1C scenes covering the investigated lakes were acquired. Details of the image information (date and cloud cover) and match-up procedure can be found in Table SII. Level-1C images were processed using the ESA Sentinel Application Platform (SNAP) version 8.0. In the following study, an average of 3×3 pixels centered at each *in situ* sampling site was employed. The BOA reflectance products were compared with the *in situ* measured Rrs using spectral response functions centered at 443, 490, 560, 665, 704, and 740 nm (Table SI).

F. Atmospheric Correction Processors

The ac process compensates for the water-leaving reflectance signals and removes the contribution of atmospheric effects [46]. The TOA reflectance is integrated by water signals, Rayleigh reflectance in the absence of aerosols, aerosol reflectance, and radiance emerging from Rayleigh-aerosol multiple scattering according to Gordon and Wang (1994) [26]. In this study, we focused on the performance evaluation of developed ac processors, e.g., Sen2Cor (08.08.00-win64), C2RCC (SNAP 8.0), iCOR (Image correction for atmospheric effects 3.0, previously called OPERA, Sterckx et al., 2015), Acolite (Atmospheric correction for OLI 'lite, py_win20211124.0, from http://odnature.naturalsciences.be/remsem/software-and-data/acolite; Polymer (v4.13) from https://www.hygeos.com/polymer, SeaWiFS Data Analysis System (SeaDas/l2gen,

TABLE III
ATTRIBUTES OF AC PROCESSORS USED TO PROCESS MSI MATCHUPS

Attributes	Sen2Cor	C2RCC (nets and C2X)	iCOR	Acolite	Polymer	SeaDas/l2gen	6S
Principles	NA	ANN, Hydrolight, and NOMAD data	Adjacency correction prior	Dark spectrum fitting and exponential extrapolation	Spectral matching method.	The 2 band multi scattering algorithm with relative humidity based model selection and iterative NIR correction	Absolute radiometric correction based on physical models
Step	1.LUT generated from libRadtran 2.Resampling of spectra	The corresponding water reflectance values are found	1. Remove Rayleigh and gaseous absorption 2. Aerosol contribution is estimated	1. Remove Rayleigh and gaseous absorption 2. Aerosol contribution is estimated	1. Remove Rayleigh and gaseous absorption 2. Aerosol contribution is estimated	1. Remove Rayleigh and gaseous absorption 2. Aerosol contribution is estimated	1. Remove Rayleigh and gaseous absorption 2. Aerosol contribution is estimated
Developed by	NA	Brockman consult[30]	VITO Sterckx et al., 2015 [52]	RBINS Vanhellemont et al., 2019[34]	HYGEOS Steinmetz et al., 2011[61]	NASA Franz et al., 2015 [61]	Vermote et al., (1996)[62]
Designed for	Land	Waters	Land/inland waters	Waters	Waters	Waters	Land
Sun-glint	NA	NA	Subtraction of minimum	Fit to residuals at Rayleigh-corrected reflectance at 1609 and 2200 nm (Gordon et al., 1988)	Treated as bulk signal	Optional	NA
Sky-glint	NA	NA	Haan and Kokke, 1996		NA	Ahmad et al., 1982	NA
Adjacency correction	NA	NA	SIMEC algorithm Sterckx et al., (2014)	NA	NA	NA	NA
Aerosol	DDV	SOS atmospheric parameters, O_3, WV, NO_2, O2, etc.	Dark target and AOT multi parameter inversion	Dark target approach	Polynomial fitting	NIR-SWIR band ratio	Aerosol component parameters, including moisture content, soot, dust, etc.
Rayleigh LUT	LibRadtran radiative transfer model	NA	MODTRAN	6SV	SOS	Ahmad et al., 1982[63]	SHARM, DISORT, and MODTRAN
AOT	The integrated extinction coefficient over a vertical column of atmosphere of unit cross section	Coastal - AERONET-OC	MODTRAN rural models	Continental/maritime aerosols	NA	Coastal/ Ocean	AOT of 550 nm or by meteorological visibility conversion
Cloud masking	NA	IdePix	The B1 band threshold	The closest wavelength (1600 nm) was selected for the nonwater masking	NA	The wavelength (865 nm) of reflectivity was selected as clound masking	NA
Water vapor retrieval (WV)	Atmospheric pre corrected differential absorption at Sentinel-2 B8a, and B9	NA	NA	NA	NA	NA	NA
Radiative transfer equation	Scene classification algorithm, LibRadtran	Hydrolight simulations	MODTRAN 5	MODTRAN 5	NA	NA	6S
Input	Native MSI	Resampled 10 m	Native MSI	Native MSI	10, 20, 60 m	Native MSI	Native MSI
Output Res. (m)	10, 20, 60	10	10, 20, 60	10	10, 20, 60 m	20, 30 m	10, 20, 60 m
Output reflectance	Bottom-Of-Atmospheric reflectance	Normalized water leaving reflectance	Bottom-Of-Atmospheric reflectance	Bottom-Of-Atmospheric reflectance	Bottom-Of-Atmospheric reflectance	Bottom-Of-Atmospheric reflectance	Bottom-Of-Atmospheric reflectance

V7.5.2.1-l2gen9.3.0), and 6S. A complete description of the ac methods is presented in Table III. For a given sun-view geometry, sensor characteristics, atmospheric conditions, and surface reflectance, the 6S model is a robust radiative transfer code to derive the surface reflectance product [47], [48]. To reduce aerosol contributions, Acolite and iCOR processors use terrestrial heritage algorithms [49], whereas SeaDas/l2gen applies the heritage ocean color approach [39]. To compensate for both aerosol and sun glint signals concurrently, the Polymer processor fits a second-order polynomial function to the Rayleigh reflectance. Likewise, for the atmospheric correction of MSI images, the Sentinel toolset includes Sen2Cor and C2RCC processors. The Sen2Cor processor is designed for land by extracting atmospheric characteristics as well as auxiliary data such as the digital elevation model and look-up tables (LUT) from the LibRadtran radiance simulation module [33]. The machine learning C2RCC processor was built upon a previous ac database of radiative transfer simulations and related TOA, relying on a per-pixel artificial neural network (ANN) [30]. It has two models with different application circumstances for open oceanic (C2RCC-nets, clear) and inland waters (C2RCC-C2X, turbid). C2X is a version of optically complex water using a 5-component bio-optical model that may be more suitable for complex inland waters.

G. Performance Indicators and Statistical Analysis

The following statistics were used to evaluate the performance of the ac processors: root mean squared error (RMSE), mean absolute error (MAE), and R^2 (determination coefficient of regression analysis) with a 45°1:1 line, for corrected ρ_s (satellite-derived aquatic reflectance) and ρ_w (*in situ* aquatic reflectance). Correlation (t-test, 2-tailed; note with **, $p < 0.01$; *, $p < 0.05$) and regression analyses were also conducted to compare and examine the relationships of different variations. r represents the correlation coefficient of the Pearson correlation analysis.

III. Results

A. Field Radiometry and Surrounding Water Quality

A total of 296 valid match-ups from 25 lakes in China and their averaged reflectance spectra from each lake are shown in Fig. 3(d). The highest averaged reflectance was observed in the lake samples from CH(18) and HZ(17), respectively. The bio-optical properties of optically complex lakes are subject to great uncertainty related to changing water quality parameters. We have measured the relative contributions of CDOM, phytoplankton, and nonalgal particles to total nonwater light absorption at 440 nm for these investigated lakes. According to the optical classification of surface waters [64], the relative contribution of collected water samplings could be classified as "CDOM-type," "nonalgal particles type (NAP-type)," and "phytoplankton-type (Phy-type)." Based on Fig. 2, it can be seen that HZ(17) lakes were NAP-type lakes, indicating that the optical contribution was dominated by nonalgal particles. The bio-optical parameters are more important and ρ_{w} increases with increasing TSM in case-II waters. The TSM of CH(18) was relatively small but the mean Chl-a value was relatively highest (range: 10.4–121 μg L^{-1}, mean: 37.09 μg L^{-1} with SD was 33.2 μg L^{-1}). This indicating that there was spatial heterogeneity for CH samples, because of eutrophic status and frequent algal bloom previously found in Lake Chaohu [22]. The TSM of HZ(17) had a large range and high mean TSM (range: 32–164 mg L^{-1}, mean: 84.20 mg L^{-1}), which could attributing to increased nonwater light absorption and particulate backscattering coefficient considering the bio-optical properties of optically complex lakes. Typical lakes with dominant nonalgal particles of optically active substances have reflectances that are very similar in shape and value. The following lakes were rich in phytoplankton, therefore having the 705 nm peak: CH(18), HZ(17), GY(16), XM(3), LM(15), and WLSU(13).

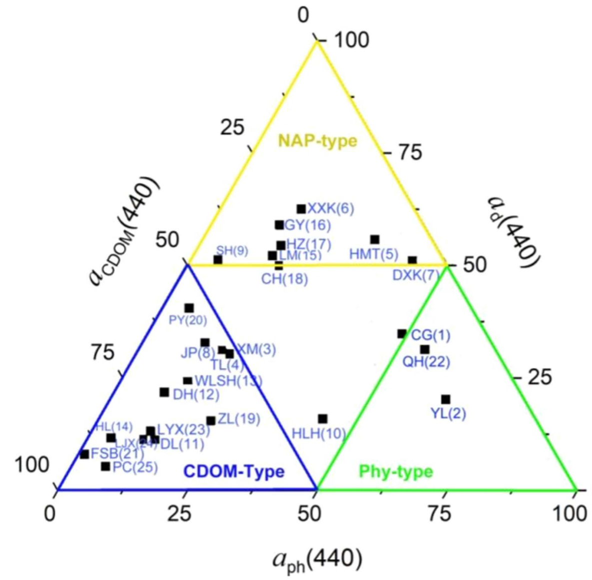

Fig. 2. Optical classification of the investigated lakes.

The concentrations of optically active substances in the 25 studied lakes across China are presented in Fig. 3(a)–(c). Because of the geological and climatic settings, the differences in [Chl-a] ($F = 13.37$, $p < 0.001$), [TSM] ($F = 9.63$, $p < 0.001$), and $a_{\mathrm{CDOM}}(440)$ ($F = 140.63$, $p < 0.001$) between lake properties were statistically significant. The relatively highest values of average [Chl-a] were measured in CH(18) (37.09 µg L^{-1} ± 34.99) with the largest level being 120.99 µg L^{-1}, indicating an algal bloom condition; the lowest values of average [Chl-a] were found in plateau lake HL(14) (0.20 µg L^{-1} ± 0.14) with the lowest level being 0.03 µg L^{-1}. Likewise, relatively lower average [TSM] was observed in PC(25) (0.40 mg L^{-1} ± 0.02), and a high [TSM] in TL(4) (86.37 mg L^{-1} ± 18.37). Subsequently, $a_{\mathrm{CDOM}}(440)$, representing CDOM levels, is usually used as a proxy for dissolved organic carbon in most inland waters [50]. It is worth mentioning that, for all lake samples, YL(2) (4.13 m^{-1} ± 1.96) showed high CDOM levels and QH(22) (0.03 m^{-1}± 0.04) the lowest.

B. Performance Evaluation of ACs for Single Lake: An Example

Atmospheric correction of inland waters is one of the major remaining challenges in aquatic remote sensing, often hindering the quantitative retrieval of biogeochemical variables and analysis of their spatial and temporal variability within aquatic environments [3]. To evaluate the performance of acs for a single lake, we collected samples from CG1 in spring (May 26th), summer (July 18th and August 18th), and autumn (September 17th). During sample collection, clear and cloudless weather conditions were selected for sampling, and the time window was ±7 days. CG1 has high variability in suspended matter, algal abundance, and trophic status (Fig. S1). All measurements in this lake were synchronized with satellite overpasses, and we aimed to test against ac processors to find the best-performing

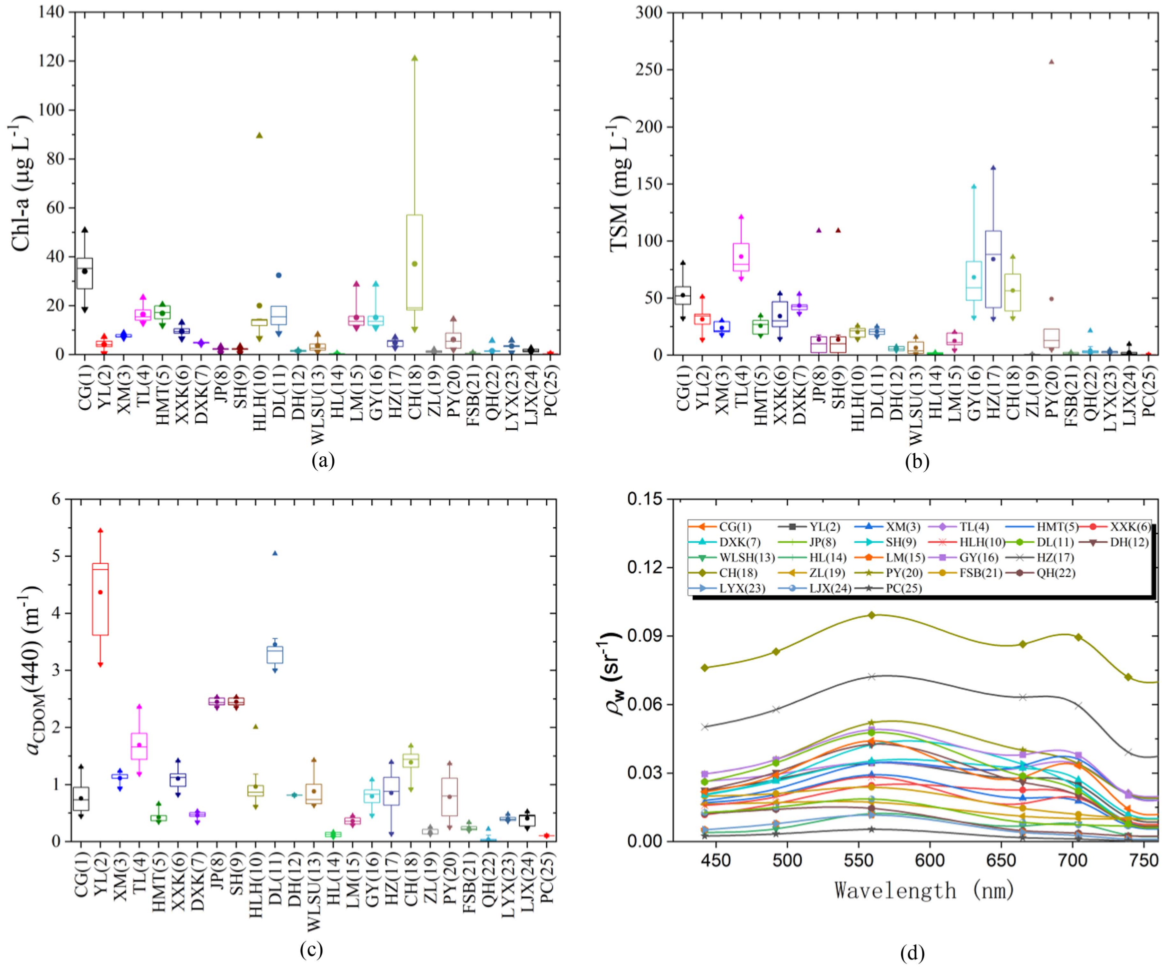

Fig. 3. Field reflectance spectra (ρw) was resampled into Sentinel-2 bands from investigated lakes.

processor based on errors and R^2. For a single lake, the match-up results between *in situ* radiometry and corrected MSI imagery showed that the evaluated acs overestimated ρ_w (Fig. 4). Considering all bands, C2RCC and Polymer processors performed better than other acs, with Polymer having relatively small errors.

C. Performance Evaluation of ACs for Lake Groups in a Large-Scale Observation

1) Performance Evaluation of Band Match-Ups for Individual AC Processors: To offer a straightforward assessment of individual performance, scatter plots for well-known ac processors from image-derived ρ_s tested against *in situ* ρ_w are shown in Fig. 5(a), including the statistical metric (fitting R^2 and errors) [Fig. 5(b)]. Overall, each processor performed differently for different MSI bands when evaluated against *in situ* and match-ups; C2RCC-nets, C2RCC-C2X, and Polymer performed better, with C2RCC returning minimal biases. Likewise, Sen2Cor, Acolite, and 6S overestimated ρ_w for the imagery and *in situ* match-ups in bands 1–6, including iCOR overestimation in the red-NIR bands. When comparing the various match-ups, nearly all ac processors showed band-dependent performance (increasing or worsening from blue to red). The limited performance in the blue (band 1:443 nm and band 2:490 nm) and red edge (band 6, 740 nm) bands, as well as the better performance in the other bands, were confirmed by all ac processors.

For the blue band (band 1:443 nm) and green band (band 2:560 nm), the performances of the Acolite and Polymer were superior when verified against *in situ* measurements. This might be partly because the majority of our data were collected in these spectral areas, which normally have greater signal intensities. C2RCC-nets and Polymer also exhibited small biases. Assuming a 30% error requirement for ρ_w, the reflectance match-ups from the Polymer processor appeared to provide valid performance at 560, 665, and 740 nm.

2) Performance Evaluation of Common Match-Ups Among Different AC Processors: The performances of match-ups for every ac were described for all valid match-ups, enabling a performance intercomparison. The match-up results (Fig. 6) show that Sen2Cor, iCOR, Acolite, and 6S produced high uncertainties and overestimations, as well as underestimation performances of C2RCC-nets and Polymer processors. Across diverse datasets and bands, C2RCC (C2X) and SeaDas/l2gen demonstrated good agreement, with a high R^2 and slope near 1. The Polymer ($R^2 = 0.28$, slope $= 0.56$) and C2RCC-C2X

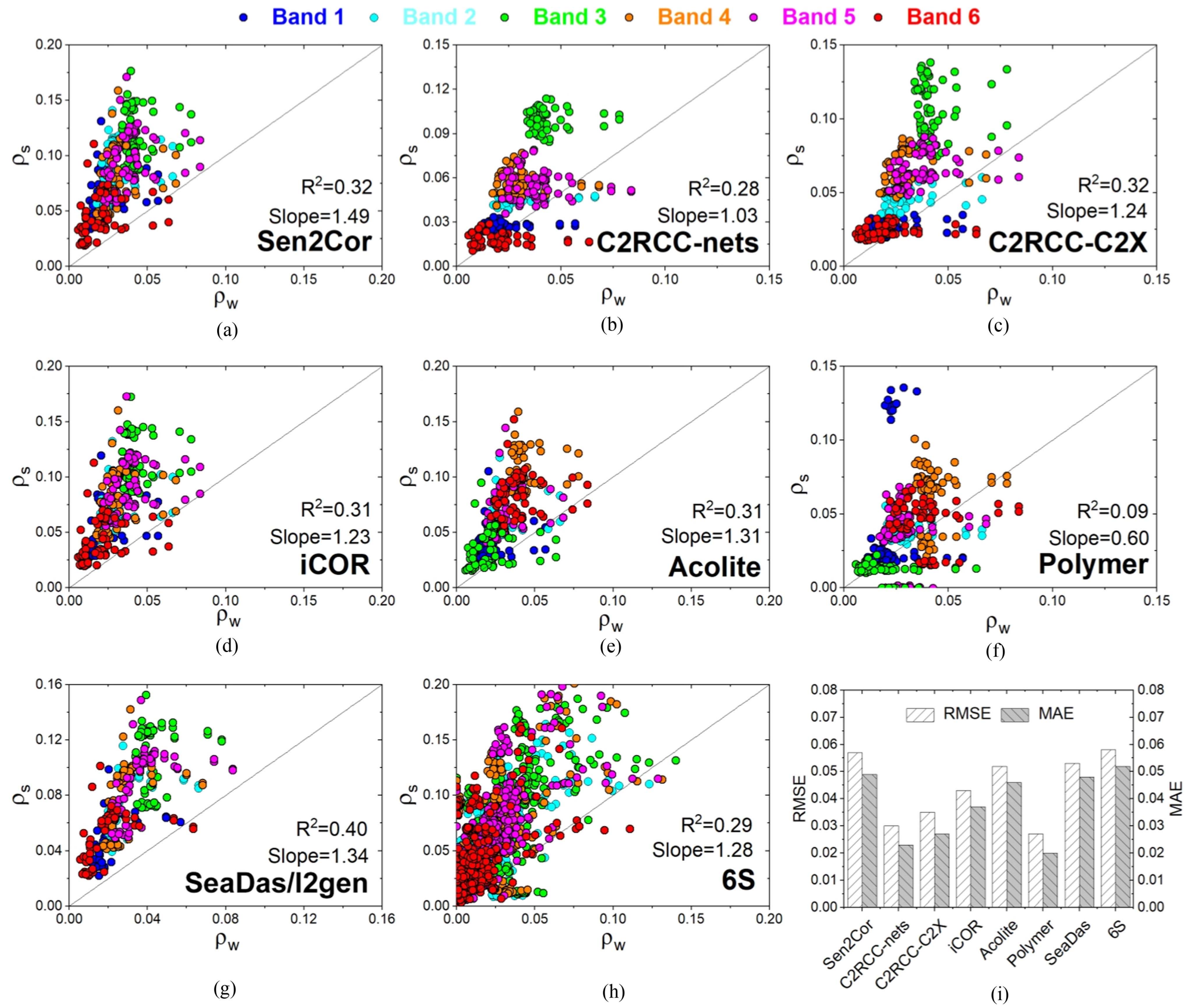

Fig. 4. Comparison of *in situ* measured reflectance spectra versus Sentinel-2A MSI reflectance spectra (band1 to band 6) of different acs (a) Sen2Cor, (b) C2RCC-nets, (c) C2RCC-C2X, (d) iCOR, (e) Acolite, (f) Polymer, (g) SeaDas/l2gen, (h) 6S and their errors, and (i) CG1.

($R^2 = 0.36$, slope $= 0.90$) with smaller errors were relatively accurate and reliable for some individual band match-ups (Fig. 5). Nevertheless, C2RCC-C2X showed the smallest errors, with RMSE and MAE being 0.027 and 0.019, respectively. The plots show that C2X is the best-performing ac method, considering all MSI bands.

IV. Discussion

A. Multispatial-Temporal in Situ Water Qualities and Sentinel-2 Data

Validation of the ac processor is important for developing derived algorithms for turning satellite imagery into quantitative and dynamic research. Our large-scale investigation of lakes across China provided abundant *in situ* ρ_w data of water qualities and optical properties (Figs. 2 and S2), as well as the additional and annual continuous sample collections recorded in CG1 (Fig. S1; [TSM], F $= 88.627$, $p < 0.001$; [Chl-a], F $= 122.933$ $p < 0.001$; $a_{\mathrm{CDOM}}(440)$, F $= 10.09$, $p < 0.001$). The time windows of ground and satellite images could affect the results because the water properties may change, for example, because of heavy rain or emerging algal blooms that change water properties in hours rather than days. Ocean color validation protocols allow a time difference of $\pm$ 2 or $\pm$ 3 h between sampling and satellite overpass; however, a ± 7 time window was accepted for the large-scale region [43], [44], [45]. On the other hand, the selection of imagery mainly depended on the required water quality. [TSM] and [Chl-a] were more easily affected by runoff via soil leaching by rainfall events, and CDOM was a relatively stable parameter (compared with the spatiotemporal variability of phytoplankton biomass). Cardille et al. (2013) [51] found that, in some cases, even longer (weeks to month scale) time differences may still be acceptable (Table SI). Many lakes, such as Peng Co in Tibet, are hard to reach, and Sentinel-2 satellites overpasses were not as frequent as in many other places. Therefore, it is difficult to plan fieldwork simultaneously with

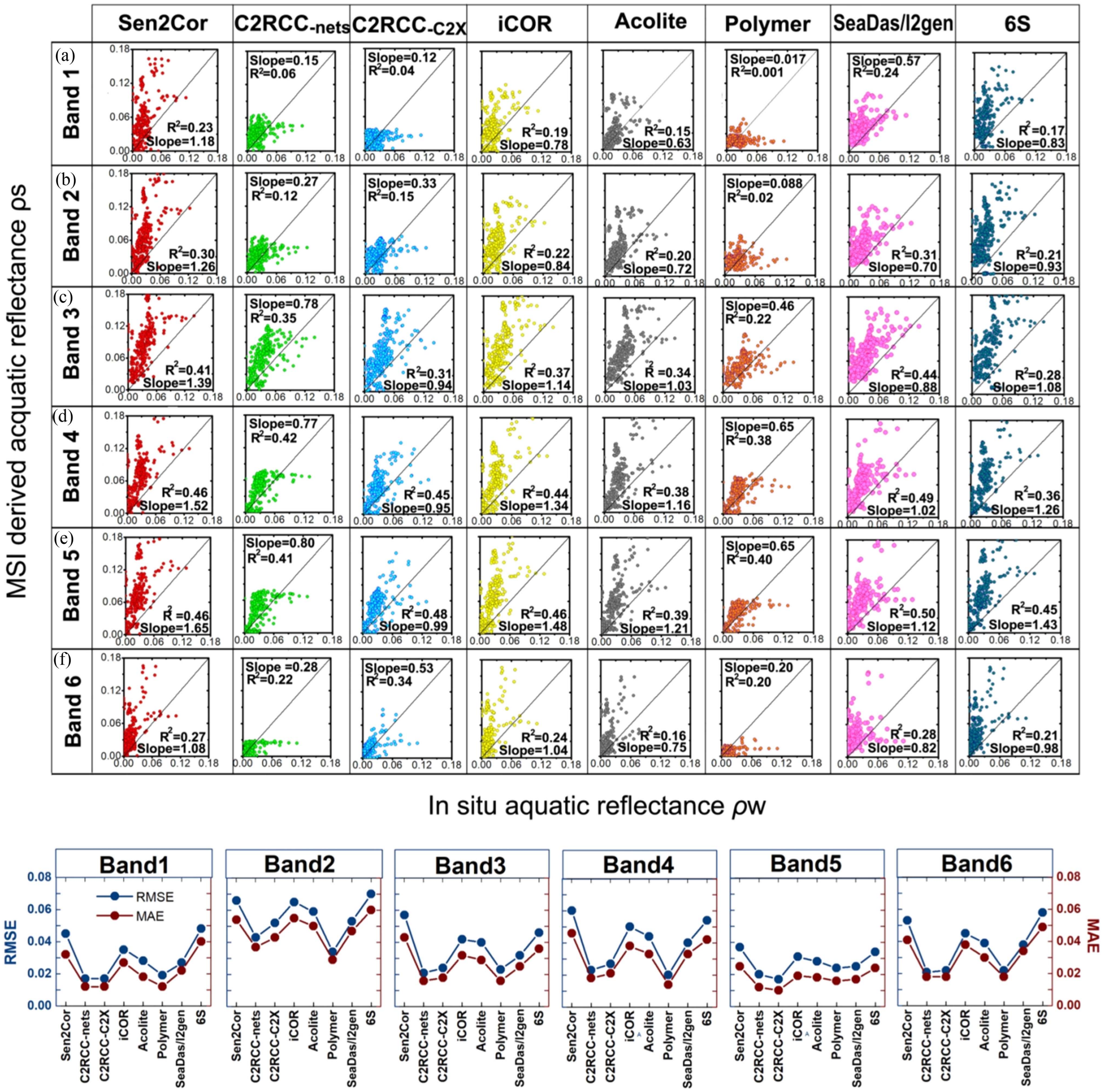

Fig. 5. Comparison of *in situ* measured reflectance spectra versus Sentinel-2A MSI reflectance spectra (band 1 to band 6) of different acs (Sen2Cor, C2RCC-nets, C2RCC-C2X, iCOR, acolite, polymer, SeaDas/l2gen, and 6S) for (a) lake groups and (b) their errors. The wavelength of MSI bands was 443 nm (band 1), 490 nm (band 2), 560 nm (band 3), 665 nm (band 4), 705 nm (band 5), and 740 nm (band 6). The black line is 1:1 line.

the satellite overpasses. Environmental conditions are stable, and anthropogenic impacts are minimal or negligible. Therefore, we expect that the results obtained do not suffer from the time difference between the *in situ* sampling and satellite overpasses.

B. AC Processors

Over 90% of the signal measured by satellites above water bodies originate from the atmosphere and does not provide any information about the water body. The final downstream science products achieved by the retrieval algorithms were dominated by accurate BOA reflectance or leaving water reflectance during the preprocessing of satellite imagery. However, neighboring considerations, such as proximity to terrestrial sources of aerosols and adjoining terrestrial topography, which result in an optically heterogeneous atmosphere, may complicate the removal of atmospheric effects over inland waterways [12]. Because multiple scattering from neighboring pixels can contribute to reflectance signals, the water-leaving radiance in the NIR region is generally not insignificant [52]. For example, in the desert, marine, and rural aerosol models, variances in the Vis bands for dazzling snow and ice surfaces are 2%, but the urban aerosol model results in a 5%–10% reflectance increase [53].

Several efforts have been made to develop ac processors to remove redundant atmospheric signals for inland waters over the past 40 years. It is also noticeable that none of the processors consistently fulfill the 30% accuracy requirements [7]. Field-measured reflectance data were used to test the performance of

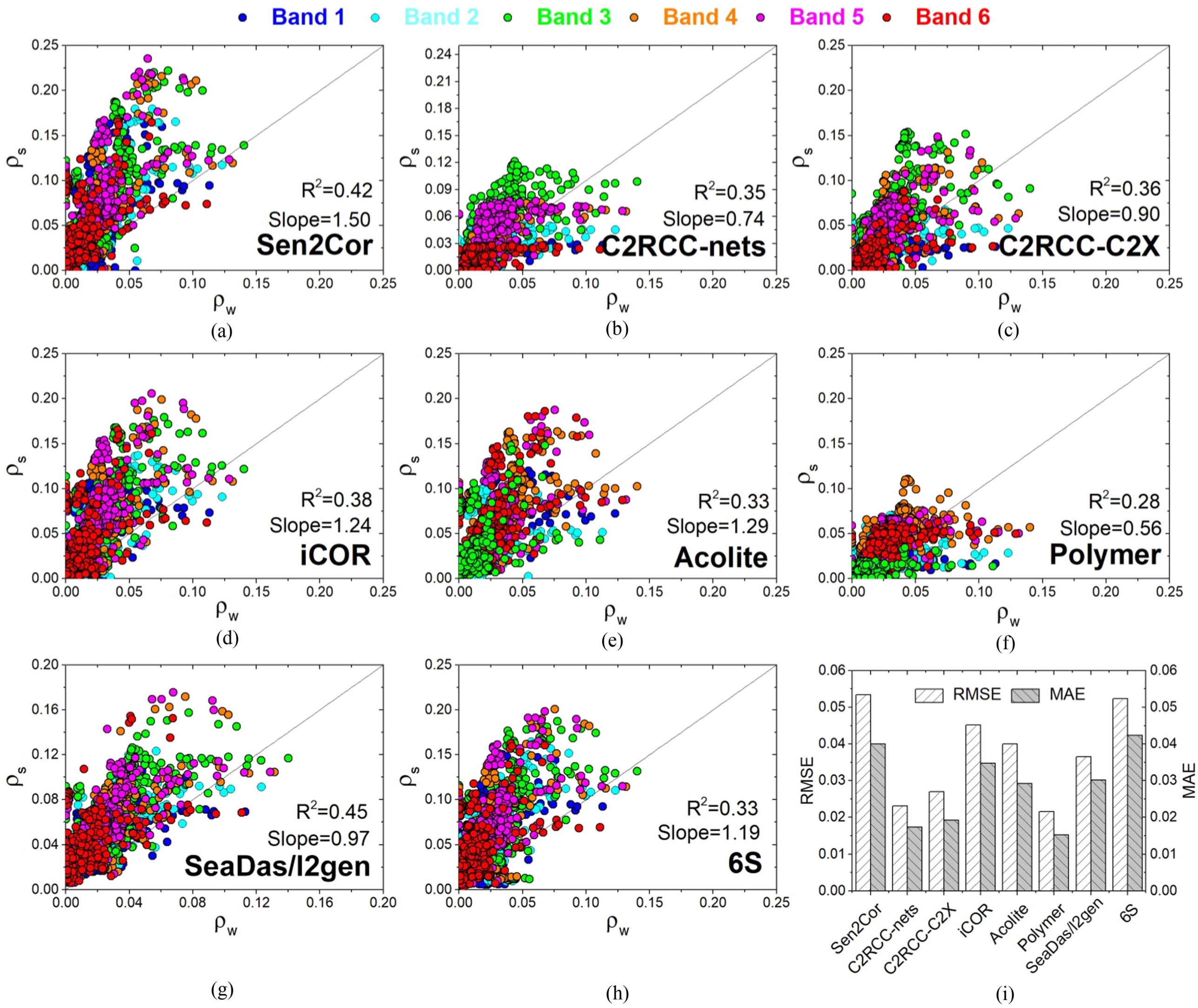

Fig. 6. Comparison of *in situ* measured reflectance spectra versus Sentinel-2A MSI reflectance spectra by different acs and their errors for lake groups, i.e., (a) Sen2Cor, (b) C2RCC-nets, (c) C2RCC-C2X, (d) iCOR, (e) Acolite, (f) Polymer, (g) SeaDas/l2gen, (h) 6S, and (i) errors. The black line is 1:1 line.

several ac processors (Fig. 3). All tested ac processors reproduced reflectance values in the right ranges, but none of them performed well over all spectral bands (Figs. 3 and 4). Most processors struggled in the 430–490 nm (B1 and B2) spectral range, and several of them (Sen2Cor, Acolite, iCOR, and 6S) had high residual signals in the NIR region of the spectrum. This is probably because of glint (Figs. 2 and 3). It should be highlighted that because of the low removal efficiency of path radiance by aerosols, all atmospheric correction processors were less efficient for inland waters in the NIR bands. These differences between the ac processors and *in situ* radiometric measurements were caused by the ac processors' integrated LUTs, parameter retrieval regarding WV content, aerosol type, or different adjacency correction algorithms, as well as the interaction of these components (Table III). Additionally, alternative radiative transfer models, such as MODTRAN 5, 6SV, and LibRadtran, have been used to build LUTs, resulting in performance differences.

Our dataset contained large variability in altitude, environmental characteristics, and landscapes (Fig. 1), which could influence the estimation of aerosol optical thickness (AOT). Therefore, relatively high uncertainties were expected in the aerosol models. Interestingly, the processors (C2RCC and Polymer) designed for water performed relatively better than the other ac processors, and Polymer generally had smaller errors (Fig. 4). This is consistent with the validations of Warren et al. (2019) [13] and Soomets et al. (2019) [24]. The C2RCC-C2X processor with the neural network algorithm achieved the highest spectral angle for lakes, followed by the net version, with a coefficient of determination and slope close to 1 (Fig. 5). The C2RCC processor (i.e., nets and C2X) was developed for waters employing neural networks while considering Hydrolight bio-optical simulations. This is most probably because C2X, an extreme version of C2RCC, had a wider train range, but the lakes under investigation in this study fit the ranges. The objective of the ESA project "Extreme Case-2 Waters" (C2X processor) is to implement water constituent retrieval in extremely turbid/productive Case-2 waters. On the other hand, Sen2Cor, iCOR, and Acolite processors showed relatively poorly underestimated reflectance in the tested lakes (Figs. 3 and 4). Some of these may be caused by land-based methodologies that generate land scene characteristics with a pixel distribution (Table III). Polynomial fitting of Polymer processor was applied for aerosol removal as part of the Rayleigh contribution removal.

The cloud detection and scene categorization theory are used in the Sen2Cor processor, as well as the dense dark vegetation (DDV) of AOT, which is adapted to the atmospheric correction of land scenes (Table III). Similarly, the iCOR processor attempts to determine the AOT using the spectral variability of land pixels in a scene. This means that good performance for the iCOR processor requires suitable variation and distribution of land pixels. Otherwise, the default value of AOT was used (Table III). The Acolite processor is designed for coastal and inland waters. The aerosol reflectance was calculated in two bands from the images after Rayleigh correction using the technique selected for the parameters. In the correction procedure, Acolite used a dark spectrum fitting approach to fit the different aerosol models. The aerosol reflectance of the other bands was extrapolated using an exponential function [33]. The Acolite processor does not employ adjacency correction, but it considers the requirement for dark pixels from shadowy land pixels, which contributes to reflectance contamination. Conversely, a spectral matching physical model-based Polymer processor was designed to process oceanic waters with and without sun glint [54]. In general, this processor had quality flags, but unlike C2RCC, it could apply all the spectral bands to make atmospheric corrections, excluding NIR signals. However, the lakes in our research region are at varying altitudes, ranging from 17 to 4000 m. Variations in altitude can cause uncertainties in estimating aerosol content within different atmospheric columns. Pahlevan et al. (2017) [46] stated that if aerosol characteristics are not properly represented in aerosol models, there would be significant uncertainties. The weak performance of the Acolite processor, together with that of other processors (e.g., Sen2Cor, iCOR), could be related to the variable lake altitudes. Highly turbid waters and macrophyte growth could also add an adjacency effect [49]. Consequently, atmospheric correction methods are needed, such as the second simulation of the satellite signal in the solar spectrum (6S) processor, which requires additional parameters to simulate the influence of the atmosphere [4]. Although the 6S processor used different atmospheric (MLW model) and aerosol models, our results also show discrete and overestimated validation for large-scale validation (Fig. 4). This is related to the imagery and regional AOT. However, the lack of local atmospheric parameters limits further analysis. As a result, more information about the altitudes of different lakes within a scene, together with their locations and LUT updates, should be considered.

C. AC Implications for Large-Scale Observations Using MSI

High spatial, temporal, and radiometric resolutions and three additional near-infrared (NIR) bands certainly make MSI sensors more powerful in identifying lake water quality; they also use alternative algorithms for retrieval [20]. Likewise, at 440 nm, the MSI signal-to-noise ratio is 40% greater than that of OLI, and aggregated MSI sensor bands might produce reasonably smooth and radiometric quality reflectance outputs (i.e., 490, 560, and 665 nm) [46]. This confirms that MSI has the potential to map [Chl-a] [21] and the synthetic trophic status index [22] to evaluate the trophic status of lakes, as well as the CDOM levels with reflectance at 440 nm [23]. However, our results for ac processors showed uneven performances for MSI (Figs. 3 and 4), indicating a challenge in acquiring accurate water-leaving reflectance signals for all bands (Vis-NIR). The results provided insight into the extent to which processors might act on the observation requirements, despite the fact that some are still in development and are not fully described. During the past several decades, limnology has benefited from remote sensing, which allows for the collection and mapping of water quality [55]. In particular, large-scale observations of water quality can track spatiotemporal patterns and have aroused wide attention [56], [57], [58]. This could help to better understand the future prospects of the lake ecosystem in response to global change. However, suitable ac processors are needed to evaluate the feasibility of transferring from a single lake to lake groups that are widely distributed. This reflects the spatiotemporal variations in match-ups for ac processors in the CG1 (Fig. 4). In particular, when all bands were pooled together, C2RCC-C2X and Polymer gave better performance, and C2X worked weakly for the signal band (Fig. 4). The performance of acs should be tested before generating accurate water-leaving reflectance and downstream products for different lakes. Pahlevan et al. (2021) [7] investigated the best performers across distinct optical water types (OWTs) as part of a joint NASA-ESA project that evaluated available ac processors for Landsat-8 and Sentinel-2 data. These results and the uncertain analysis provided by Pahlevan et al. (2021) [7] can guide satellite users to select relatively good ac processors considering OWTs. However, for lake groups in large-scale observations, it is time- and computation-consuming, requiring accurate water-leaving reflectance, including science products.

As stated in Section IV-B, these ac processors may perform differently, and it is always difficult to achieve a unified good performance. Hence, we collected the multispatial-temporal *in situ* water quality data across China, including various characteristics of optical water absorption contribution and trophic status (Fig. 3). The Polymer processor performed best and provided small errors in the sensitive bands responding to water quality (Fig. 6) when all bands were pooled together. Nevertheless, for the signal band, the Polymer processor worked better for every band (bands 1–6) than the C2RCC processor for Chinese lakes. These results indicate that, if we used a signal band or a combination of empirical models to map downstream products, such as red and NIR bands for [Chl-a] [21] and Green/Red bands [59] for CDOM, both are recommended. Considering the increased usage of machine learning algorithms [22], all visible bands seem to be used as input variables in models and could show robust performance [60]. We also evaluated the applicable efficiency of a typical CG1 (Table SIII), occupying MSI scene imagery. In contrast, a Polymer processor could save more storage space, instead of time, than C2RCC.

V. Conclusion

Our study tested several atmospheric correction processors and documented them using Sentinel-2A/B large-scale data for different lake types in China. Our findings include the followings:

1) Water qualities, that is, [Chl-a], [TSM], and CDOM, showed significant differences in a large-scale region.
2) C2RCC and Polymer processors performed best for all band match-ups with *in situ* field radiometry, and the latter could work better when considering empirical algorithms.
3) For large-scale observations, the Polymer processor is recommended for quantifying water quality when all bands are pooled together.

Most evaluated atmospheric correction processors (Sen2Cor, C2RCC, Acolite, Polymer, iCOR, SeaDas/l2gen, and 6S) have some limitations, comparable with one another. The findings of this study indicate that effective selection of an atmospheric correction processor for MSI imagery can provide intercompatibility for monitoring dynamic water quality and downstream products.

Acknowledgment

The authors would like to thank all staff and students for their persistent assistance with both field sampling and laboratory analysis.

References

[1] V. Sagan et al., "Monitoring inland water quality using remote sensing: Potential and limitations of spectral indices, bio-optical simulations, machine learning, and cloud computing," *Earth-Sci. Rev.*, vol. 205, 2020, Art. no. 103187.

[2] L. Guanter et al., "Atmospheric correction of ENVISAT/MERIS data over inland waters: Validation for European lakes," *Remote Sens. Environ.*, vol. 114, no. 3, pp. 467–480, 2010.

[3] V. Martins et al., "Assessment of atmospheric correction methods for Sentinel-2 MSI images applied to Amazon floodplain lakes," *Remote Sens.*, vol. 9, no. 4, p. 322, 2017.

[4] G. Doxani et al., "Atmospheric correction inter-comparison exercise," *Remote Sens.*, vol. 10, no. 2, p. 352, 2018.

[5] A. N. Tyler et al., "Developments in Earth observation for the assessment and monitoring of inland, transitional, coastal and shelf-sea waters," *Sci. Total Environ.*, vol. 572, pp. 1307–1321, 2016.

[6] N. Liu et al., "Evaluation and comparison of multiangle implementation of the atmospheric correction algorithm, dark target, and deep blue aerosol products over China," *Atmos. Chem. Phys.*, vol. 19, no. 12, pp. 8243–8268, 2019.

[7] N. Pahlevan et al., "ACIX-aqua: A global assessment of atmospheric correction methods for Landsat-8 and Sentinel-2 over lakes, rivers, and coastal waters," *Remote Sens. Environ.*, vol. 258, 2021, Art. no. 112366.

[8] C. Jamet et al., "Comparison of three SeaWiFS atmospheric correction algorithms for turbid waters using AERONET-OC measurements," *Remote Sens. Environ.*, vol. 115, no. 8, pp. 1955–1965, 2011.

[9] M. Wang and L. Jiang, "Atmospheric correction using the information from the short blue band," *IEEE Trans. Geosci. Remote Sens.*, vol. 56, no. 10, pp. 6224–6237, Oct. 2018.

[10] D. Müller et al., "The ocean colour climate change initiative: I. A methodology for assessing atmospheric correction processors based on in-situ measurements," *Remote Sens. Environ.*, vol. 162, pp. 242–256, 2015.

[11] M. H. Tavares et al., "Atmospheric and sunglint correction for retrieving chlorophyll-a in a productive tropical estuarine-lagoon system using Sentinel-2 MSI imagery," *ISPRS J. Photogrammetry*, vol. 174, pp. 215–236, 2021.

[12] W. J. Moses et al., "Atmospheric correction for inland waters," in *Bio-Optical Modeling and Remote Sensing of Inland Waters*. Amsterdam, The Netherlands: Elsevier, 2017, pp. 69–100.

[13] M. Warren et al., "Assessment of atmospheric correction algorithms for the Sentinel-2A multispectral imager over coastal and inland waters," *Remote Sens. Environ.*, vol. 225, pp. 267–289, 2019.

[14] M. A. Warren et al., "Complementary water quality observations from high and medium resolution Sentinel sensors by aligning chlorophyll-a and turbidity algorithms," *Remote Sens. Environ.*, vol. 265, 2021, Art. no. 112651.

[15] G. S. Okin et al., "The impact of atmospheric conditions and instrument noise on atmospheric correction and spectral mixture analysis of multispectral imagery," *Remote Sens. Environ.*, vol. 164, pp. 130–141, 2015.

[16] J. Bramich et al., "Improved red-edge chlorophyll-a detection for Sentinel 2," *Ecol. Indicators*, vol. 120, 2021, Art. no. 106876.

[17] C. Cairo et al., "Hybrid chlorophyll-a algorithm for assessing trophic states of a tropical Brazilian reservoir based on MSI/Sentinel-2 data," *Remote Sens.*, vol. 12, no. 1, p. 40, 2019.

[18] T. Harmel et al., "Sunglint correction of the multi-spectral instrument (MSI)-SENTINEL-2 imagery over inland and sea waters from SWIR bands," *Remote Sens. Environ.*, vol. 204, pp. 308–321, 2018.

[19] A. H. Pickens et al., "Global seasonal dynamics of inland open water and ice," *Remote Sens. Environ.*, vol. 272, 2022, Art. no. 112963.

[20] K. Toming et al., "First experiences in mapping lake water quality parameters with Sentinel-2 MSI imagery," *Remote Sens.*, vol. 8, no. 8, p. 640, 2016.

[21] S. Li et al., "Quantification of chlorophyll-a in typical lakes across China using Sentinel-2 MSI imagery with machine learning algorithm," *Sci. Total Environ.*, vol. 778, 2021, Art. no. 146271.

[22] S. Li et al., "Mapping the trophic state index of Eastern lakes in China using an empirical model and Sentinel-2 imagery data," *J. Hydrol.*, vol. 608, 2022, Art. no. 127613.

[23] H. Gordon et al., "A semianalytic radiance model of ocean color," *J. Geophys. Res.–Ocean.*, vol. 93, pp. 10909–10924, 1988.

[24] T. Soomets et al., "Comparison of lake optical water types derived from Sentinel-2 and Sentinel-3," *Remote Sens.*, vol. 11, no. 23, 2019, Art. no. 2883.

[25] F. Gascon et al., "Copernicus Sentinel-2A calibration and products validation status," *Remote Sens.*, vol. 9, no. 6, p. 584, 2017.

[26] H. R. Gordon et al., "Retrieval of water-leaving radiance and aerosol optical thickness over the oceans with SeaWiFS: A preliminary algorithm," *Appl. Opt.*, vol. 33, no. 3, pp. 443–452, 1994.

[27] J. H. Ahn et al., "Simple aerosol correction technique based on the spectral relationships of the aerosol multiple-scattering reflectances for atmospheric correction over the oceans," *Opt. Express*, vol. 24, no. 26, pp. 29659–29669, 2016.

[28] B. C. Gao et al., "Atmospheric correction algorithms for hyperspectral remote sensing data of land and ocean," *Remote Sens. Environ.*, vol. 113, pp. S17–S24, 2009.

[29] H. Wu et al., "Rapid transformation of ambient absorbing aerosols from West African biomass burning," *Atmos. Chem. Phys.*, vol. 21, no. 12, pp. 9417–9440, 2021.

[30] C. Brockmann et al., "Evolution of the C2RCC neural network for Sentinel 2 and 3 for the retrieval of ocean colour products in normal and extreme optically complex waters," in *Proc. Living Planet Symp.*, 2016, vol. 740, p. 54.

[31] A. Ansper et al., "Retrieval of chlorophyll a from Sentinel-2 MSI data for the European Union water framework directive reporting purposes," *Remote Sens.*, vol. 11, no. 1, p. 64, 2018.

[32] C. O. Ilor et al., "Analyzing performances of different atmospheric correction techniques for Landsat 8: Application for coastal remote sensing," *Remote Sens.*, vol. 11, no. 4, p. 469, 2019.

[33] M. Pereira-Sandoval et al., "Evaluation of atmospheric correction algorithms over Spanish inland waters for Sentinel-2 multi spectral imagery data," *Remote Sens.*, vol. 11, no. 12, 2019, Art. no. 1469.

[34] Q. Vanhellemont et al., "Adaptation of the dark spectrum fitting atmospheric correction for aquatic applications of the Landsat and Sentinel-2 archives," *Remote Sens. Environ.*, vol. 225, pp. 175–192, 2019.

[35] C. E. Binding et al., "EOLakeWatch; delivering a comprehensive suite of remote sensing algal bloom indices for enhanced monitoring of Canadian eutrophic lakes," *Ecol. Indicators*, vol. 121, 2021, Art. no. 106999.

[36] B. A. Schaeffer et al., "An initial validation of Landsat 5 and 7 derived surface water temperature for US lakes, reservoirs, and estuaries," *Int. J. Remote Sens.*, vol. 39, no. 22, pp. 7789–7805, 2018.

[37] R. Ma et al., "China's lakes at present: Number, area and spatial distribution," *Sci. China Earth Sci.*, vol. 54, no. 2, pp. 283–289, 2011.

[38] C. D. Mobley et al., "Estimation of the remote-sensing reflectance from above-surface measurements," *Appl. Opt.*, vol. 38, no. 36, pp. 7442–7455, 1999.

[39] C. D. Mobley et al., "Polarized reflectance and transmittance properties of windblown sea surfaces," *Appl. Opt.*, vol. 54, no. 15, pp. 4828–4849, 2015.

[40] S. T. Jeffrey et al., "New spectrophotometric equations for determining chlorophylls a, b, c1 and c2 in higher plants, algae and natural phytoplankton," *Biochemie und Physiologie der Pflanzen*, vol. 167, no. 2, pp. 191–194, 1975.

[41] M. Babin et al., "Variations in the light absorption coefficients of phytoplankton, nonalgal particles, and dissolved organic matter in coastal waters around Europe," *J. Geophys. Res.*, vol. 108, no. C7, 2003.

[42] M. Drusch et al., "Sentinel-2: ESA's optical high-resolution mission for GMES operational services," *Remote Sens. Environ.*, vol. 120, pp. 25–36, 2012.

[43] K. Song et al., "Quantification of lake clarity in China using Landsat OLI imagery data," *Remote Sens. Environ.*, vol. 243, 2020, Art. no. 111800.

[44] N. Sriwongsitanon et al., "Influence of atmospheric correction and number of sampling points on the accuracy of water clarity assessment using remote sensing application," *J. Hydrol.*, vol. 401, no. 3/4, pp. 203–220, 2011.

[45] E. J. Tebbs et al., "Remote sensing of chlorophyll-a as a measure of cyanobacterial biomass in Lake Bogoria, a hypertrophic, saline–alkaline, flamingo lake, using Landsat ETM+," *Remote Sens. Environ.*, vol. 135, pp. 92–106, 2013.

[46] N. Pahlevan et al., "Sentinel-2 multispectral instrument (MSI) data processing for aquatic science applications: Demonstrations and validations," *Remote Sens. Environ.*, vol. 201, pp. 47–56, 2017.

[47] E. F. Vermote et al., "Atmospheric correction of visible to middle-infrared EOS-MODIS data over land surfaces: Background, operational algorithm and validation," *J. Geophys. Res.-Atmos.*, vol. 102, no. D14, pp. 17131–17141, 1997.

[48] E. F. Vermote et al., "Atmospheric correction for the monitoring of land surfaces," *J. Geophys. Res.-Atmos.*, vol. 113, no. D23, 2008.

[49] L. De Keukelaere et al., "Atmospheric correction of Landsat-8/OLI and Sentinel-2/MSI data using iCOR algorithm: Validation for coastal and inland waters," *Eur. J. Remote Sens.*, vol. 51, no. 1, pp. 525–542, 2018.

[50] C. G. Griffin et al., "Quantifying CDOM and DOC in major arctic rivers during ice-free conditions using Landsat TM and ETM+ data," *Remote Sens. Environ.*, vol. 209, pp. 395–409, 2018.

[51] J. A. Cardille et al., "Remote sensing of lake CDOM using noncontemporaneous field data," *Can. J. Remote Sens.*, vol. 39, no. 2, pp. 118–126, 2013.

[52] S. Sterckx et al., "OPERA: An atmospheric correction for land and water," in *Proc. Sentinel-3 Sci. Workshop*, 2015, vol. 1, pp. 3–6.

[53] M. König et al., "Application of Sentinel-2 MSI in arctic research: Evaluating the performance of atmospheric correction approaches over arctic sea ice," *Front. Earth Sci.*, vol. 7, p. 22, 2019.

[54] HYGEOS. Polymer, Accessed: Dec. 01, 2018. [Online]. Available: https://www.hygeos.com/polymer

[55] T. Kutser et al., "Remote sensing of shallow waters–A 50 year retrospective and future directions," *Remote Sens. Environ.*, vol. 240, 2020, Art. no. 111619.

[56] X. Hou et al., "Global mapping reveals increase in lacustrine algal blooms over the past decade," *Nature Geosci.*, vol. 15, no. 2, pp. 130–134, 2022.

[57] S. Wang et al., "A dataset of remote-sensed forel-ule index for global inland waters during 2000–2018," *Sci. Data*, vol. 8, no. 1, pp. 1–10, 2021.

[58] Y. Zhang et al., "Remote sensing estimation of water clarity for various lakes in China," *Water Res.*, vol. 192, 2021, Art. no. 116844.

[59] T. Kutser et al., "Mapping lake CDOM by satellite remote sensing," *Remote Sens. Environ.*, vol. 94, no. 4, pp. 535–540, 2005.

[60] Z. Cao et al., "A machine learning approach to estimate chlorophylla from Landsat-8 measurements in inland lakes," *Remote Sens. Environ.*, vol. 248, 2020, Art. no. 111974.

[61] F. Steinmetz et al., "Atmospheric correction in presence of sun glint: Application to MERIS," *Opt Express*, vol. 19, no. 10, pp. 9783–9800, 2011.

[62] E. Vermote et al., "Radiative transfer modelling for calibration and atmospheric correction," in *Advances in the Use of NOAA AVHRR Data for Land Applications*, 1996, pp. 49–72.

[63] Z. Ahmad et al., "An iterative radiative transfer code for ocean-atmosphere systems," *J. Atmos. Sci.*, vol. 39, no. 3, pp. 656–665, 1982.

[64] L. Prieur et al., "An optical classification of coastal and oceanic waters based on the specific spectral absorption curves of phytoplankton pigments, dissolved organic matter, and other particulate materials," *Limnology Oceanogr.*, vol. 26, no. 4, pp. 671–689, 1981.

Sijia Li received the Ph.D. degree in environmental science from Northeast Normal University, Changchun, China, in 2020.

From 2018 to 2020, she was a visiting Ph.D. student with Estonian Marine Institute, Tartu University. She is currently an Assistant Research Fellow of Environmental Remote Sensing Applications with NEIGAE, Chinese Academy of Sciences, Changchun, China. She is working on inland water qualities dynamics, particularly focused on inland lake wetlands with respect to anthropogenic and climate driving forces. Her research interests include water optics, hyperspectral remote sensing, and GIS spatial analysis.

Kaishan Song received the M.S. degree in GIS and cartography from Northeast Normal University, Changchun, China, in 2002, and the Ph.D. degree in remote sensing application from Northeast Institute of Geography and Agroecology (IGA), Chinese Academy of Sciences (CAS), Changchun, China, in 2005.

He is currently a Full Professor for Remote Sensing of Environment Applications with IGA, CAS. His research interests include bio-optical properties of inland waters, remote sensing of water quality, and impact of climatic and anthropogenic driving forces on water quality spatiotemporal variations with remotely sensed imagery data.

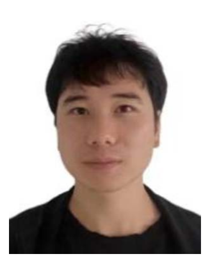

Yong Li received the B.S. degree in surveying and mapping engineering, and the M.S. degree in civil and hydraulic engineering from the University of Science and Technology Liaoning, Anshan, China, in 2019 and 2023, respectively.

He is a staff in Northeast Institute of Geography and Agroecology (IGA), Chinese Academy of Sciences (CAS), Changchun, China, from 2023. His research interests include water optics, atmospheric correction algorithm, and water quality parameters.

Ge Liu received the B.S. degree in geographic science from Liaocheng University, Liaocheng, China, in 2011, and the Ph.D. degree in environmental remote sensing from Nanjing Normal University, Nanjing, China, in 2017.

He is currently with the Northeast Institute of Geography and Agricultural Ecology, Chinese Academy of Sciences, Changchun, China. His research interests include water color remote sensing and optical properties in optically complex water bodies.

Zhidan Wen received the B.S. degree in bioengineering from Northeast Forestry University, Harbin, China, in 2007, the M.S. degree in microbiology from Shenyang Agricultural University, Shenyang, China, in 2010, and the Ph.D. degree in environmental science and engineering from the Harbin Institute of Technology, Harbin, China, in 2014.

She is currently with the Northeast Institute of Geography and Agroecology, Chinese Academy of Sciences, Changchun, China. Her research interests include carbon cycle in water and greenhouse gas emissions from inland water bodies.

Lili Lyu received the master's degree in inorganic chemistry from the College of Chemistry, Northeast Normal University, Changchun, China, in 2011. She is currently working toward the Ph.D. degree in cartography and geographic information system with the Northeast Institute of Geography and Agroecology, Chinese Academy of Sciences, Changchun, China.

Her research interests include water quality parameters, eutrophic status, water optical parameters, etc.

Yingxin Shang received the B.S. degree in environmental science from the Changchun University of Science and Technology, Changchun, China, in 2012, and the Ph.D. degree in cartography and geographic information system from the University of Chinese Academy of Sciences, Beijing, China, in 2020.

She is currently with the Northeast Institute of Geography and Agroecology, Chinese Academy of Sciences, Changchun, China. Her research interests include CDOM and optical properties in optically complex water bodies.

Chong Fang received the Ph.D. degree from the University of Chinese Academy of Sciences, Beijing, China, in 2020.

From 2020 to 2022, she worked as a Postdoctoral with Dalian University of Technology. She is currently an Associate Researcher of the project in Environmental Remote Sensing Applications with NEIGAE, Chinese Academy of Sciences, Changchun, China. Her research interests include remote estimating of algal blooms, water quality parameters, etc.